Supramolecular Functionalization of Single-Walled Carbon Nanotubes with Conjugated Polyelectrolytes and Their Patterning on Surfaces

Fuyong Cheng,[†,||] Patigul Imin,[†,||] Sorin Lazar,[||,‡] Gianluigi A. Botton,[||,‡] Glynis de Silveira,[||,⊥] Ognian Marinov,[§] Jamal Deen,[§] and Alex Adronov*[,†,||]

Department of Chemistry, Department of Materials Science and Engineering, Department of Electrical and Computer Engineering, Brockhouse Institute for Materials Research, and The Canadian Centre for Electron Microscopy, McMaster University, Hamilton, Ontario, Canada

Received September 22, 2008; Revised Manuscript Received October 28, 2008

ABSTRACT: The interaction between single-walled carbon nanotubes and two anionic conjugated polyelectrolytes, poly[2,5-bis(3-sulfonatopropoxy)-1,4-phenylene-*alt*-1,4-phenylene) sodium salt and poly[2,5-bis(3-sulfonatopropoxy)-1,4-ethynylphenylene-*alt*-1,4-ethynylphenylene] sodium salt, was investigated. It was found that the supramolecular polymer−nanotube assembly occurred efficiently and produced stable complexes that could be purified from excess free polymer in solution. These complexes were characterized using absorption spectroscopy, fluorescence spectroscopy, Raman spectroscopy, and electron microscopy. It was further found that patterning of these polymer−nanotube complexes could be accomplished by utilizing electrostatic attraction with a prepatterned, cationically charged surface. Patterned features were found to be electrically conducting with a measured sheet resistance value of 0.68 ± 0.01 MΩ for features having a thickness on the order of several nanometers.

Introduction

The unique structural, mechanical, and electronic properties of single-walled carbon nanotubes (SWNTs) have placed these materials center stage within nanoscience communities. Specifically, the high electron mobilities[1] and current densities[2] that SWNTs can sustain make them promising for use as molecular wires in nanoscale electrical circuitry. Coupled to their mechanical robustness, these electronic properties also make SWNTs viable candidates for a wide array of flexible plastic electronics. SWNTs have already been implemented within a variety of devices, including chemical sensors, field-effect transistors, nanoscale integrated radio receivers,[3,4] photovoltaics, and field-emission sources. In most of these and other applications, the precise, reproducible, rapid, and scalable positioning, orientation, and patterning of individual SWNTs on nanometer-to-micron length scales are integral to their function. However, SWNT patterning over large areas in a reliable and convenient manner continues to be an extremely challenging endeavor.

Recent effort in the area of nanotube patterning has resulted in successful methods for nanotube alignment on surfaces using Langmuir−Blodgett techniques,[5,6] external field-assisted filtration and deposition methods,[7−9] and capillary-flow-induced orientation of nanotubes as a result of droplet drying.[10,11] The generation of nanotube patterns on surfaces was also initially accomplished through the patterned deposition of catalysts for nanotube growth in predefined regions on a Si/SiO_2 surface by chemical vapor deposition (CVD),[12,13] resulting in a highly controlled spatial distribution of nanotube forests. However, this solid-state technique requires high temperature, is limited in substrate compatibility, and is not generally accessible. In terms of solution-phase patterning, the use of inkjet printing,[14,15] microfluidic techniques (coupled to controlled flocculation),[16,17] and electrospinning/fiber deposition methods have also resulted in patterned carbon nanotubes.[18] Although effective, each of these solution-phase techniques requires specialized equipment, involves complicated nanotube formulations/processing, and produces patterns in a serial method that precludes the large-scale, high-throughput fabrication of nanotube patterns.

An alternative strategy for nanotube patterning involves the self-assembly of appropriately functionalized nanotubes on prepatterned surfaces. Prepatterning can involve the deposition of amine groups (known to induce binding of oxidatively purified nanotubes through acid−base chemistry) by microcontact printing (MCP), dip-pen nanolithography (DPN), and electron beam lithography or by surface charging using an atomic force microscope (AFM).[17,19−25] Similarly, patterning of biomolecules, such as DNA, has been shown to induce the self-assembly of nanotubes in patterns dictated by electrostatic and specific base-pairing interactions.[26,27] Additionally, the selective binding of nanotubes covalently functionalized with organic acids (hydroxamic acid) to lithographically patterned basic metal oxides has resulted in the fabrication of patterned, aligned nanotube devices with high spatial resolution.[28−30] Although these methods allow parallel, high-throughput fabrication of nanotube patterns, it can be argued that the complexity of the required equipment, nanotube functionalization, and limited surface compatibility may hinder the widespread adoption of these techniques.

In an attempt to develop a simple, easily accessible method for nanotube patterning using inexpensive, readily available starting materials and equipment, we have focused our attention on the supramolecular functionalization of carbon nanotubes with conjugated polyelectrolytes (CPEs).[31−35] Recently, it has been shown that conjugated polymers form strong supramolecular interactions with SWNTs, enabling their dissolution in organic solvents.[36−44] In the case of CPEs, the conjugated polymer backbone should result in nanotube binding behavior similar to that of their nonionic counterparts with the added benefit of imparting excellent aqueous solubility and the possibility for self-assembly through electrostatic interactions (i.e., layer-by-layer assembly). In addition, CPEs exhibit interesting optoelectronic properties, making them potentially

* Corresponding author. Address: Department of Chemistry, McMaster University, 1280 Main Street West, Hamilton, ON, L8S 4M1. Tel: (905) 525-9140, ext. 23514. Fax: (905) 521-2773. E-mail: adronov@mcmaster.ca.
† Department of Chemistry.
‡ Department of Materials Science and Engineering.
§ Department of Electrical and Computer Engineering.
|| Brockhouse Institute for Materials Research.
⊥ The Canadian Centre for Electron Microscopy.

10.1021/ma802147s CCC: $40.75
Published on Web 11/20/2008

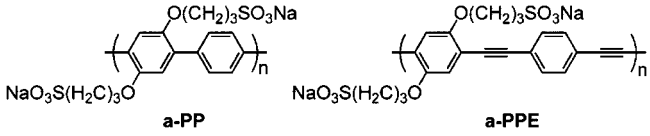

Figure 1. Chemical structures of the two CPEs used for nanotube functionalization.

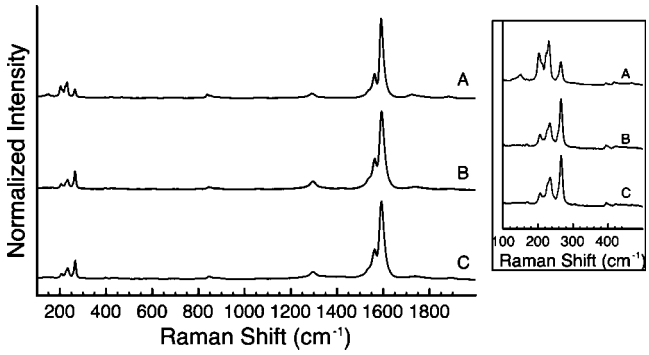

Figure 2. Raman spectra of (A) pristine SWNTs, (B) a-PP-functionalized SWNTs, and (C) a-PPE-functionalized SWNTs. Inset at right shows a magnified view of the radial breathing mode signals between 100 and 300 cm^{-1}.

useful in a variety of device applications, such as light-emitting diodes,[33] photovoltaic cells,[35] and sensors.[32] Despite these advantages, noncovalent functionalization of carbon nanotubes with CPEs has received little attention. Here we report that noncovalent functionalization of SWNTs with water-soluble CPEs is possible and allows selective patterning via electrostatic interactions among SWNTs functionalized with an anionic CPE on a photolithographically prepatterned cationic surface.

Results and Discussion

Two anionic CPEs, derivatives of poly(phenylene) and poly(phenylene ethynylene), were investigated. Both poly[2,5-bis(3-sulfonatopropoxy)-1,4-phenylene-*alt*-1,4-phenylene) sodium salt (a-PP)[31] and poly[2,5-bis(3-sulfonatopropoxy)-1,4-ethynylphenylene-*alt*-1,4-ethynylphenylene] sodium salt (a-PPE)[34] were synthesized according to literature methods. (For structures, see Figure 1.) Considering the rigid-rod conjugated backbone of both a-PP and a-PPE, we postulated that these polymers would exhibit strong $\pi-\pi$ stacking interactions with the surface of SWNTs. Furthermore, because the interaction would take place in water, it was expected that hydrophobic interactions between the nanotubes and the polymer backbone would additionally aid and strengthen their assembly.

To investigate the interactions between carbon nanotubes and the two CPEs, a mixture of as-received HiPco SWNTs (10 mg), obtained from Carbon Nanotechnologies, and either a-PP or a-PPE (30 mg) in 20 mL of deionized water was sonicated for 20 min. This produced a homogeneous solution that was then filtered through a 200 nm pore diameter Teflon membrane and was repeatedly washed with water to remove the excess free polymer (as determined from the disappearance of fluorescence in the filtrate). The collected polymer−SWNT complex (black powder) was again dissolved in water by sonication for 5 min and centrifugation at 5000 rpm (2576*g*) for 20 min. The dark, clear supernatant solution was found to remain stable with no visible precipitation of nanotubes for more than 6 months. Considering that any polymer not bound to the nanotube surface had been removed, this result indicates that the supramolecular interaction between the two CPEs and SWNTs is extremely strong, with the adsorbed polymer remaining bound to the surface even when diluted with clean solvent. Gravimetric analysis of recovered free polymer from these experiments allowed an estimation of the amount of polymer that was bound to the SWNT surface in the CPE−SWNT complexes, which was approximately 27 wt % for a-PP−SWNT and 40 wt % for a-PPE−SWNT. The solution stability results can be compared with previous work in which ionic small molecules, such as pyrene and naphthalene derivatives, were adsorbed to the nanotube surface to produce water-soluble SWNT-based polyelectrolytes.[45] The previously reported small-molecule-modified SWNTs precipitate in the absence of excess free adsorbate in solution, indicating that in our case the multivalent binding of the CPE greatly increases the strength of the polymer−nanotube interaction. The stability of these solutions is likely a result of two factors: the aqueous solubility imparted by the sulfonate functionalities of the two CPEs as well as the prevention of aggregation due to the intermolecular electrostatic repulsion of these functional groups. The concentration of SWNTs within these aqueous solutions was estimated using UV/vis spectroscopy by measuring the nanotube absorbance at 500 nm according to previously published methods.[46−48] From this data, the nanotube concentration was determined to be ca. 1.8 mg/mL, regardless of which CPE adsorbate was utilized. The high nanotube concentration within these solutions is another indicator of the effectiveness of CPEs for nanotube dissolution.

The characterization of the CPE-functionalized carbon nanotubes by Raman spectroscopy revealed very little change in the signals of the SWNTs upon supramolecular functionalization (Figure 2). The spectral shift of both the graphitic G band at ~1590 cm^{-1} and the radial breathing modes (RBMs) in the range of 200−300 cm^{-1} remained relatively unchanged when compared with pristine, as-received SWNTs. The disorder (D) band at ~1300 cm^{-1} also did not significantly increase in intensity upon supramolecular functionalization, indicating that the above treatment of nanotubes with CPEs does not introduce any defects within the resulting structures. A close examination of the RBM signals, which can be used to calculate the nanotube diameter by the relationship $d = 234/\nu$ (where d is the tube

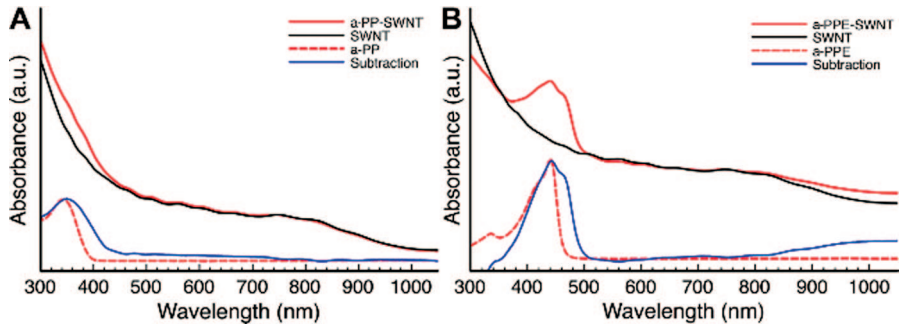

Figure 3. UV−vis-NIR absorption spectra of the free polymer, the polymer−nanotube complex, pristine SWNTs, and the polymer component of the complex for (A) a-PP and (B) a-PPE.

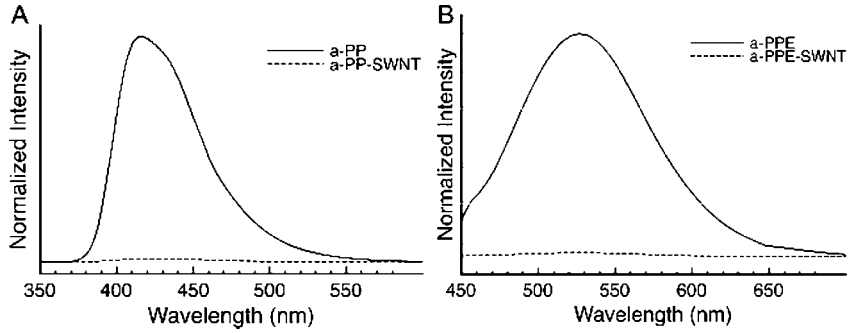

Figure 4. Normalized fluorescence spectra of free polymer (—) and the polymer—nanotube complex (---) of (A) a-PP and (B) a-PPE.

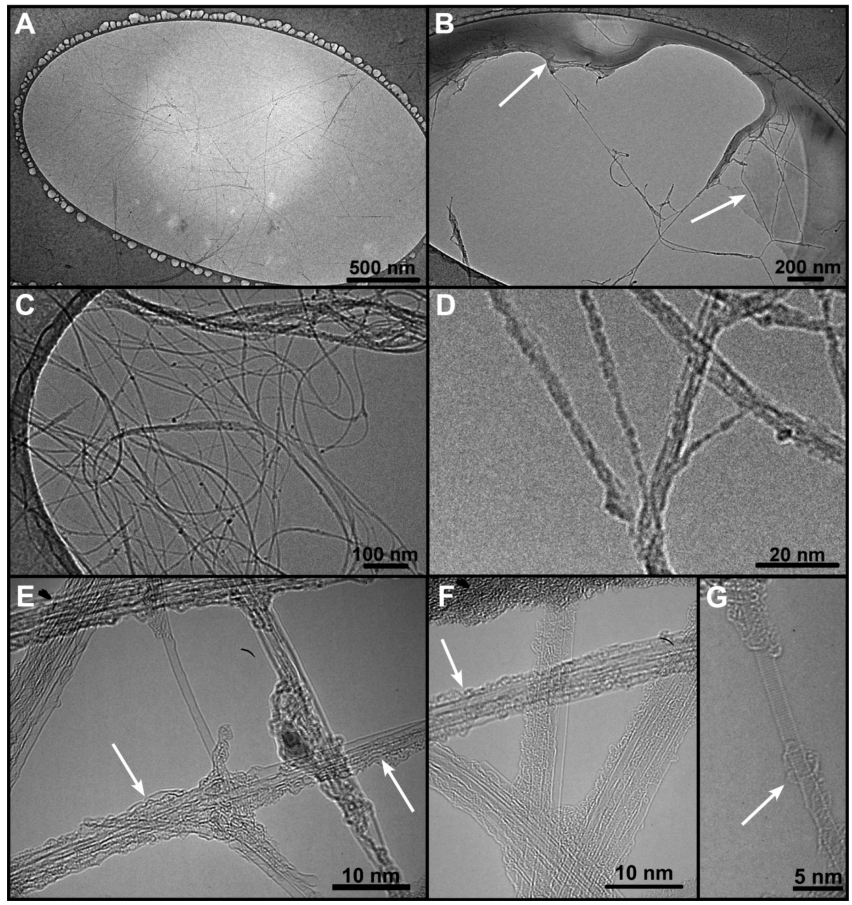

Figure 5. Cryo-TEM images of a-PP—SWNT (A) before sublimation of ice, (B) during sublimation (arrows indicate location of nanotubes still tethered to sheets of ice), and (C,D) after complete sublimation. (E—G) Ultra-high-resolution TEM images of the sample after complete sublimation of ice showing individual SWNTs, small bundles, and the surface functionalization with polymer (arrows).

diameter in nm and ν is the Raman shift of the peak in cm^{-1}),[49—51] indicates that some diameter selectivity occurs during supramolecular complexation with CPEs. Specifically, the weak signal at 150 cm^{-1} in as- received SWNTs (Figure 2A), corresponding to a nanotube diameter of ~1.5 nm, completely disappears in the spectra of the two CPE-functionalized SWNT samples (Figure 2, inset). Additionally, the signals at 200 and 230 cm^{-1} (corresponding to diameters of ~1.2 and ~1.0 nm, respectively) decrease in intensity relative to the signal at 265 cm^{-1} (corresponding to a nanotube diameter of ~0.9 nm). Together, these data indicate that there exists a preference for lower nanotube diameters to be complexed by the CPEs that were used in this study.

The UV—vis-NIR absorption spectra of the two CPEs (a-PP and a-PPE) as well as their complexes with nanotubes (a-PP—SWNT and a-PPE—SWNT) are depicted in Figure 3. In both cases, the spectrum of the polymer—SWNT complex exhibited features that corresponded to each of the respective polymers (a shoulder at ~340 and ~440 nm for a-PP and a-PPE, respectively). In both cases, the absorption spectrum of the polymer component within the polymer—SWNT complex was generated by subtracting the SWNT absorption spectrum (measured from a poly(styrene sulfonate)—SWNT (PSS—SWNT) complex where the polymer has no measurable absorption beyond 300 nm) from that of the polymer—SWNT complex, where both were normalized at 746 nm. The resulting spectrum (blue curve, labeled "Subtraction" in Figure 3) is broadened and slightly red-shifted when compared to the spectrum of the corresponding free polymer in solution. This shift and broadening is indicative of the stacking interaction that occurs between the π system of the polymer and the nanotube.

The fluorescence spectra of the CPEs show a clear and dramatic change upon polymer adsorption to the nanotube surface (Figure 4). To compare the emission spectra of the free

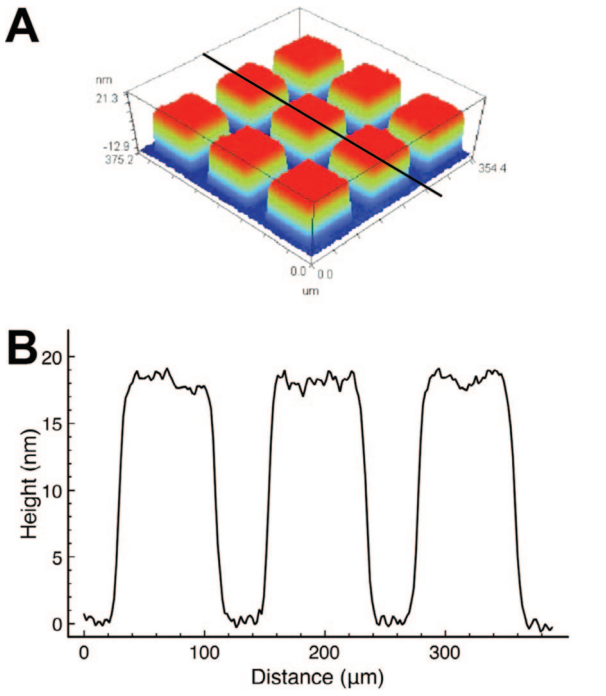

Figure 6. (A) Pattern of squares imaged by optical profilometry and formed by immersing a prepatterned glass slide with 90 μm squares of cross-linked PVMP in an aqueous solution of a-PP−SWNTs. (B) Cross-sectional height versus distance plot of the sample shown in A, where the black line indicates the location of the cross section.

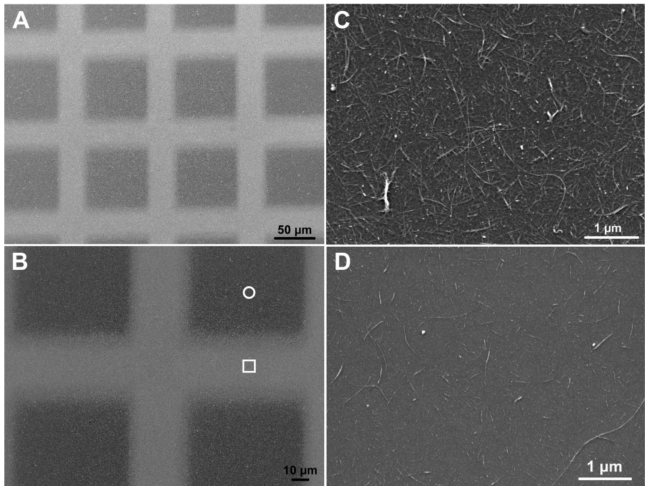

Figure 7. SEM images of patterned SWNTs on a glass substrate. (A) and (B) represent images of the substrate at two different magnifications, whereas (C) and (D) represent further magnified images of the areas marked with a white ○ and □ in image B, respectively.

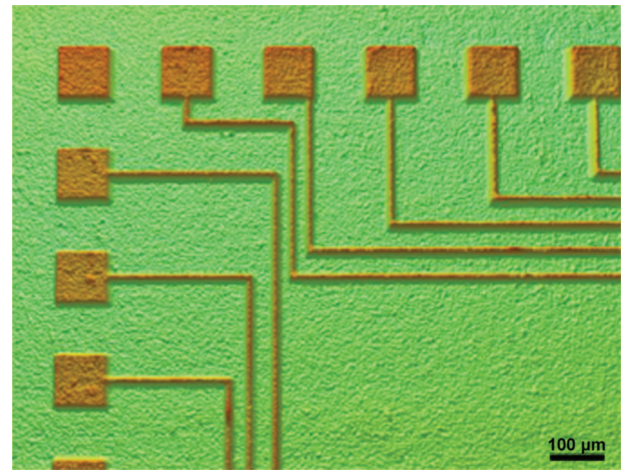

Figure 8. Optical profilometry image showing a section of a photolithographically reproduced pattern of electrodes and wires, where the features are composed of a-PPE−SWNT complexes on top of a photocross-linked PVMP pattern.

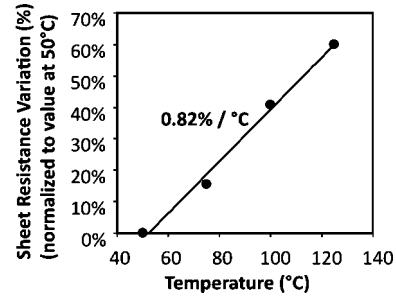

Figure 9. Temperature variation of sheet resistance.

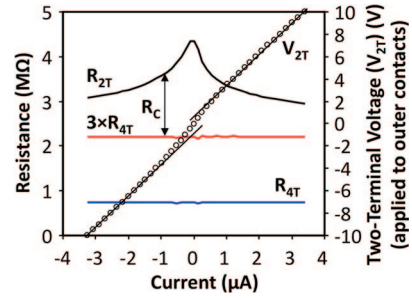

Figure 10. Variations in electrical conduction properties of a patterned SWNT film as a function of DC current flowing through the sample. The contact resistance R_C is the difference between the total sample resistance (R_{2T}) and the total film resistance ($3(R_{4T})$) between the outer contacts. The increase in R_C at low bias causes a step in the I versus V plot (○). The thin eye-guide lines are drawn through the circles to illustrate the step.

polymer and its nanotube-bound counterpart quantitatively, we corrected the emission spectra using a multiplication factor obtained from the normalization of their corresponding absorption spectra, as previously described.[44] From this data, it is clear that significant quenching of polymer emission (in excess of 98%) occurs upon polymer−nanotube complex formation, which is likely a result of photoinduced electron or energy transfer from the polymer to the nanotube.[39,52−56]

Microstructural characterization of the polymer−nanotube complexes was accomplished by cryogenic transmission electron microscopy (cryo-TEM) in aqueous solution.[57−59] The advantage of cryo-TEM in this analysis is that it provides a picture of nanotube morphology in solution (albeit frozen) rather than within a dried sample on a TEM grid. In the latter case, nanotubes are generally aggregated, which prevents any conclusions on the degree of exfoliation of nanotubes by the appended polymer. Conversely, by rapidly freezing an aqueous solution of polymer-functionalized nanotubes, it is possible to view the sample as it exists in solution in the absence of external driving forces for aggregation. Figure 5A−D depicts a series of cryo-TEM images of an a-PP−SWNT sample taken before and after the sublimation of the ice in which the sample was suspended. This was accomplished by allowing the sample to warm up slowly from −192 to −170 °C under high vacuum. While embedded in the ice, the contrast between the nanotubes and the ice was relatively low (Figure 5A). However, during sublimation, the nanotubes became clearly visible as intertwined strands anchoring sections of ice prior to its disappearance

(Figure 5B, arrows). After sublimation, the majority of the strands appeared as individual fibers with some forming small bundles (Figure 5C,D). Subsequently, a high-resolution TEM analysis of the same sublimated sample was also performed at room temperature using an 80 keV electron beam, which enables imaging of both the nanotubes and polymer adsorbates while minimizing damage to the sample (Figure 5E,F). The high-resolution images clearly show the presence of individual tubes as well as small bundles of tubes that are coated with polymer chains, as indicated by arrows in Figure 5E,F.

Patterned nanotube films were produced by directing the electrostatic adsorption of a-PP- and a-PPE-functionalized SWNTs on a prepatterned, positively charged poly-4-vinyl-*N*-methylpyridine (PVMP) layer, which was produced via photochemical cross-linking, as previously described.[60] In a typical experiment, a glass microscope coverslip was spin-coated with a 95% ethanol solution of PVMP (0.5 wt %) followed by 1 h of irradiation with 254 nm light (using a hand-held UV lamp), where one part of the surface was covered with a 200 mesh TEM grid that served as a photomask. The exposed sample was developed with methanol and deionized water and was then immersed in an aqueous saturated solution of a-PP−SWNT or a-PPE−SWNT overnight. Deionized water was used to wash away any nonspecifically physisorbed SWNTs, and the substrate surface was visualized using an optical profilometer and scanning electron microscopy (SEM). The optical profilometry image in Figure 6 depicts a regular 3D pattern of square features (90×90 μm) on the glass surface, exactly matching the openings of the TEM grid that was used as a photomask. Cross-sectional analysis indicated that the total height of these features was ~20 nm, with the cross-linked PVMP layer making up the majority of the observed features (Figure 6B). The transparent a-PP−SWNT layer was found to make up only the topmost ca. 3 ± 0.7 nm, which is consistent with what is expected for a monolayer of individual polymer-functionalized nanotubes or small bundles of these structures. Considering that the electrostatic deposition of nanotubes is likely to result in significant amounts of overlapping tubes (and small bundles of tubes) in an interwoven network, the rough nature of the observed surface is also in reasonable agreement with the expectation.

The exact nature of the deposited nanotube features was probed by SEM. Figure 7A depicts the pattern of square features that resulted from the photochemical cross-linking of PVMP followed by the deposition of CPE-functionalized nanotubes. Clearly, the openings of the TEM grid are reproduced on the surface with high fidelity. Higher magnification images show that the interiors of the squares, which are composed of the positively charged cross-linked PVMP layer below a layer of electrostatically deposited a-PP−SWNTs, indeed contain deposited nanotubes. A dense film of interwoven nanotubes is present in all areas that were initially irradiated and cross-linked during the photolithographic step (Figure 7C). Conversely, the trenches between the patterned squares, on which the PVMP was not cross-linked and therefore washed away, contained significantly fewer nanotubes with only a small number of nonspecifically adsorbed structures that were not successfully washed away during the rinsing step (Figure 7D). These images again indicate that nanotube patterning was successfully achieved simply by the use of an inexpensive polymer, a readily available photomask, and a hand-held UV lamp.

In a further proof-of-concept experiment, a more complicated pattern used for metallization in a high-speed photodetector device (typically produced by photolithographic methods) was replicated using the same procedures as those described above. The replicated pattern, which consisted of a-PPE−SWNT complexes on a glass substrate, is depicted in Figure 8. We note that the exact reproduction of 10 μm lines was possible using this methodology. A complete optical image of the photomask pattern is available in the Supporting Information.

The electrical properties of the patterned films were also investigated. Considering that these patterns are composed of a percolation network of individual CPE-functionalized SWNTs, it was expected that the patterned features would exhibit electrical conductivity. By carefully contacting the sample with a pair of tungsten needle electrodes in a probe station and measuring the current by applying a DC voltage between the electrodes, we observed that the resistance between pads connected by the 10 μm wide patterned lines (Figure 8) is much lower than that when one of the electrodes was contacted to an unconnected feature (i.e., the square pad in the upper left corner of Figure 8). Thus, we gathered that the transparent SWNT film and patterns are continuous and successfully replicate the metallization patterns normally used in integrated circuits.

To quantify the conductivity of the SWNT patterns further, we used the aforementioned methodology to prepare a sample for four-point resistance measurements. The sample consisted of a patterned SWNT stripe that was 1.5 mm wide and several millimeters long. Four equally spaced gold contact pads were deposited on top of the sample perpendicular to the SWNT stripe with a distance of 2 mm between the pad edges. By applying a voltage sweep between the outer pads while recording the potentials of the inner pads, we measured the current flowing through the sample. (See the Supporting Information for details.) The ratio of the applied voltage to the measured current was the two-terminal resistance (R_{2T}) of the sample, and the difference between the potentials of the inner pads divided by the measured current was the four-terminal resistance (R_{4T}) of the film. From R_{4T}, it was determined that the sheet resistance of the film was in the range of 0.68 ± 0.01 MΩ at room temperature, and it increased with temperature at a rate of ~0.8%/°C (Figure 9). However, the temperature effect was negligible when compared with the larger contact resistance between the SWNT film and the gold pads, a well-documented issue that plagues SWNT devices.[61,62]

By comparing the calculated value of total film resistance ($3(R_{4T})$) with the total measured sample resistance (R_{2T}, Figure 10), which is the sum of the film and contact resistances, we estimated that the total contact resistance (R_C) is ~30−50% of the total sample resistance (R_{2T}) and is nonlinear. Additional details are provided in the Supporting Information. The contact resistance (R_C) depends on the current in the sample, owing to a Schottky barrier between the gold pads and nanotubes,[61] whereas the film resistance (R_{4T}) is bias independent. Thus, whereas we demonstrate the feasibility of the method to create fine conductive patterns, more investigations are necessary to optimize the electrical properties of the functionalized film and improve the electrical conductivity of both the film and the contacts to it.

Conclusions

Supramolecular functionalization of carbon nanotubes with CPEs leads to the formation of stable complexes that remain soluble in aqueous solution, even upon the removal of excess free polymer. UV−vis-NIR absorption measurements revealed a slight bathochromic shift and broadening of the polymer absorption spectrum, whereas fluorescence measurements showed practically quantitative fluorescence quenching of the polymer once it was adsorbed to the nanotube surface. Microstructural analysis by TEM allowed the direct visualization of exfoliated nanotube bundles that were coated with polymer. The anionic nature of the resulting complexes allowed their patterning on glass substrates via electrostatic interactions with a preformed pattern of cationic PVMP, which was prepared by photo-cross-linking thin films of the polymer through a photomask. The

patterned nanotube-containing features exhibited electrical conductivity as a result of the interpenetrated network of nanotubes, confirming the continuity of the patterned features with widths as small as 10 μm. Thus, we have demonstrated a simple, inexpensive method for creating fine conductive nanotube patterns that can be suitable for large-area electronic devices. Further investigation will be required to improve the film conductivity and methods for electrical contacting to the nanotube patterns.

Supporting Information Available: Full experimental details are provided. This material is available free of charge via the Internet at http://pubs.acs.org.

Acknowledgment. We would like to thank Professor Joaquin Ortega for help with cryo-TEM. Financial support for this work was provided by the Natural Science and Engineering Research Council (NSERC) of Canada, the Emerging Materials Knowledge program of the Ontario Centres of Excellence (OCE-EMK), the Canada Foundation for Innovation (CFI), and the Ontario Innovation Trust (OIT).

References and Notes

(1) Durkop, T.; Getty, S. A.; Cobas, E.; Fuhrer, M. S. *Nano Lett.* **2004**, *4*, 35–39.
(2) Yao, Z.; Kane, C. L.; Dekker, C. *Phys. Rev. Lett.* **2000**, *84*, 2941–2944.
(3) Jensen, K.; Weldon, J.; Garcia, H.; Zettl, A. *Nano Lett.* **2007**, *7*, 3508–3511.
(4) Rutherglen, C.; Burke, P. *Nano Lett.* **2007**, *7*, 3296–3299.
(5) Kim, Y.; Minami, N.; Zhu, W.; Kazaoui, S.; Azumi, R.; Matsumoto, M. *Synth. Met.* **2003**, *135*, 747–748.
(6) Kim, Y.; Minami, N.; Zhu, W. H.; Kazaoui, S.; Azumi, R.; Matsumoto, M. *Jpn. J. Appl. Phys., Part 1* **2003**, *42*, 7629–7634.
(7) Walters, D. A.; Casavant, M. J.; Qin, X. C.; Huffman, C. B.; Boul, P. J.; Ericson, L. M.; Haroz, E. H.; O'Connell, M. J.; Smith, K.; Colbert, D. T.; Smalley, R. E. *Chem. Phys. Lett.* **2001**, *338*, 14–20.
(8) Vijayaraghavan, A.; Blatt, S.; Weissenberger, D.; Oron-Carl, M.; Hennrich, F.; Gerthsen, D.; Hahn, H.; Krupke, R. *Nano Lett.* **2007**, *7*, 1556–1560.
(9) Makaram, P.; Selvarasah, S.; Xiong, X.; Chen, C.; Busnaina, A.; Khanduja, N.; Dokmeci, M. R. *Nanotechnology* **2007**, *18*, 395204.
(10) Xin, H. J.; Woolley, A. T. *Nano Lett.* **2004**, *4*, 1481–1484.
(11) Li, Q.; Zhu, Y. T.; Kinloch, I. A.; Windle, A. H. *J. Phys. Chem. B* **2006**, *110*, 13926–13930.
(12) Wei, B. Q.; Vajtai, R.; Jung, Y.; Ward, J.; Zhang, R.; Ramanath, G.; Ajayan, P. M. *Nature* **2002**, *416*, 495–496.
(13) Wei, B. Q.; Vajtai, R.; Jung, Y.; Ward, J.; Zhang, R.; Ramanath, G.; Ajayan, P. M. *Chem. Mater.* **2003**, *15*, 1598–1606.
(14) Kordas, K.; Mustonen, T.; Toth, G.; Jantunen, H.; Lajunen, M.; Soldano, C.; Talapatra, S.; Kar, S.; Vajtai, R.; Ajayan, P. M. *Small* **2006**, *2*, 1021–1025.
(15) Small, W. R.; Panhuis, M. i. h. *Small* **2007**, *3*, 1500–1503.
(16) Park, J. U.; Meitl, M. A.; Hur, S. H.; Usrey, M. L.; Strano, M. S.; Kenis, P. J. A.; Rogers, J. A. *Angew. Chem., Int. Ed.* **2006**, *45*, 581–585.
(17) Meitl, M. A.; Zhou, Y. X.; Gaur, A.; Jeon, S.; Usrey, M. L.; Strano, M. S.; Rogers, J. A. *Nano Lett.* **2004**, *4*, 1643–1647.
(18) Gao, J. B.; Yu, A. P.; Itkis, M. E.; Bekyarova, E.; Zhao, B.; Niyogi, S.; Haddon, R. C. *J. Am. Chem. Soc.* **2004**, *126*, 16698–16699.
(19) Liu, J.; Casavant, M. J.; Cox, M.; Walters, D. A.; Boul, P.; Lu, W.; Rimberg, A. J.; Smith, K. A.; Colbert, D. T.; Smalley, R. E. *Chem. Phys. Lett.* **1999**, *303*, 125–129.
(20) Rao, S. G.; Huang, L.; Setyawan, W.; Hong, S. H. *Nature* **2003**, *425*, 36–37.
(21) Tsukruk, V. V.; Ko, H.; Peleshanko, S. *Phys. Rev. Lett.* **2004**, *92*, 065502.
(22) Im, J.; Lee, M.; Myung, S.; Huang, L.; Rao, S. G.; Lee, D. J.; Koh, J.; Hong, S. *Nanotechnology* **2006**, *17*, 3569–3573.
(23) Wang, Y. H.; Maspoch, D.; Zou, S. L.; Schatz, G. C.; Smalley, R. E.; Mirkin, C. A. *Proc. Natl. Acad. Sci. U.S.A.* **2006**, *103*, 2026–2031.
(24) Auvray, S.; Derycke, V.; Goffman, M.; Filoramo, A.; Jost, O.; Bourgoin, J. P. *Nano Lett.* **2005**, *5*, 451–455.
(25) Seemann, L.; Stemmer, A.; Naujoks, N. *Nano Lett.* **2007**, *7*, 3007–3012.
(26) Xin, H. J.; Woolley, A. T. *J. Am. Chem. Soc.* **2003**, *125*, 8710–8711.
(27) Keren, K.; Berman, R. S.; Buchstab, E.; Sivan, U.; Braun, E. *Science* **2003**, *302*, 1380–1382.
(28) Hannon, J. B.; Afzali, A.; Klinke, C.; Avouris, P. *Langmuir* **2005**, *21*, 8569–8571.
(29) Klinke, C.; Hannon, J. B.; Afzali, A.; Avouris, P. *Nano Lett.* **2006**, *6*, 906–910.
(30) Tulevski, G. S.; Hannon, J.; Afzali, A.; Chen, Z.; Avouris, P.; Kagan, C. R. *J. Am. Chem. Soc.* **2007**, *129*, 11964–11968.
(31) Kim, S.; Jackiw, J.; Robinson, E.; Schanze, K. S.; Reynolds, J. R.; Baur, J.; Rubner, M. F.; Boils, D. *Macromolecules* **1998**, *31*, 964–974.
(32) Chen, L. H.; McBranch, D. W.; Wang, H. L.; Helgeson, R.; Wudl, F.; Whitten, D. G. *Proc. Natl. Acad. Sci. U.S.A.* **1999**, *96*, 12287–12292.
(33) Baur, J. W.; Kim, S.; Balanda, P. B.; Reynolds, J. R.; Rubner, M. F. *Adv. Mater.* **1998**, *10*, 1452–1455.
(34) Tan, C. Y.; Pinto, M. R.; Schanze, K. S. *Chem. Commun.* **2002**, 446–447.
(35) Taranekar, P.; Qiao, Q.; Jiang, H.; Ghiviriga, I.; Schanze, K. S.; Reynolds, J. R. *J. Am. Chem. Soc.* **2007**, *129*, 8958–8959.
(36) Tang, B. Z.; Xu, H. Y. *Macromolecules* **1999**, *32*, 2569–2576.
(37) Curran, S. A.; Ajayan, P. M.; Blau, W. J.; Carroll, D. L.; Coleman, J. N.; Dalton, A. B.; Davey, A. P.; Drury, A.; McCarthy, B.; Maier, S.; Strevens, A. *Adv. Mater.* **1998**, *10*, 1091–1093.
(38) Star, A.; Stoddart, J. F.; Steuerman, D.; Diehl, M.; Boukai, A.; Wong, E. W.; Yang, X.; Chung, S. W.; Choi, H.; Heath, J. R. *Angew. Chem., Int. Ed.* **2001**, *40*, 1721–1725.
(39) Chen, J.; Liu, H. Y.; Weimer, W. A.; Halls, M. D.; Waldeck, D. H.; Walker, G. C. *J. Am. Chem. Soc.* **2002**, *124*, 9034–9035.
(40) Rice, N. A.; Soper, K.; Zhou, N.; Merschrod, E.; Zhao, Y. *Chem. Commun.* **2006**, 4937–4939.
(41) Cheng, F.; Adronov, A. *Chem.—Eur. J.* **2006**, *12*, 5053–5059.
(42) Cheng, F.; Zhang, S.; Adronov, A.; Echegoyen, L.; Diederich, F. *Chem.—Eur. J.* **2006**, *12*, 6062–6070.
(43) Cheng, F.; Adronov, A. *J. Porphyrins Phthalocyanines* **2007**, *11*, 198–204.
(44) Cheng, F.; Imin, P.; Maunders, C.; Botton, G.; Adronov, A. *Macromolecules* **2008**, *41*, 2304–2308.
(45) Paloniemi, H.; Aaritalo, T.; Laiho, T.; Liuke, H.; Kocharova, N.; Haapakka, K.; Terzi, F.; Seeber, R.; Lukkari, J. *J. Phys. Chem. B* **2005**, *109*, 8634–8642.
(46) Bahr, J. L.; Mickelson, E. T.; Bronikowski, M. J.; Smalley, R. E.; Tour, J. M. *Chem. Commun.* **2001**, 193–194.
(47) Liu, Y. Q.; Yao, Z. L.; Adronov, A. *Macromolecules* **2005**, *38*, 1172–1179.
(48) Bahun, G. J.; Wang, C.; Adronov, A. *J. Polym. Sci., Part A: Polym. Chem.* **2006**, *44*, 1941–1951.
(49) Wang, J. S.; Wai, C. M.; Shimizu, K.; Cheng, F.; Boeckl, J. J.; Maruyama, B.; Brown, G. *J. Phys. Chem. C* **2007**, *111*, 13007–13012.
(50) Chiang, I. W.; Brinson, B. E.; Huang, A. Y.; Willis, P. A.; Bronikowski, M. J.; Margrave, J. L.; Smalley, R. E.; Hauge, R. H. *J. Phys. Chem. B* **2001**, *105*, 8297–8301.
(51) Chiang, I. W.; Brinson, B. E.; Smalley, R. E.; Margrave, J. L.; Hauge, R. H. *J. Phys. Chem. B* **2001**, *105*, 1157–1161.
(52) Guldi, D. M.; Rahman, G. M. A.; Zerbetto, F.; Prato, M. *Acc. Chem. Res.* **2005**, *38*, 871–878.
(53) Rahman, G. M. A.; Guldi, D. M.; Cagnoli, R.; Mucci, A.; Schenetti, L.; Vaccari, L.; Prato, M. *J. Am. Chem. Soc.* **2005**, *127*, 10051–10057.
(54) Cioffi, C.; Campidelli, S.; Sooambar, C.; Marcaccio, M.; Marcolongo, G.; Meneghetti, M.; Paolucci, D.; Paolucci, F.; Ehli, C.; Rahman, G. M. A.; Sgobba, V.; Guldi, D. M.; Prato, M. *J. Am. Chem. Soc.* **2007**, *129*, 3938–3945.
(55) Mao, J.; Liu, Q.; Lv, X.; Liu, Z.; Huang, Y.; Ma, Y.; Chen, Y.; Yin, S. *J. Nanosci. Nanotechnol.* **2007**, *7*, 2709–2718.
(56) Chawla, J. S.; Gupta, D.; Narayan, K. S.; Zhang, R. *Appl. Phys. Lett.* **2007**, *91*, 043510.
(57) Thiruvengadathan, R.; Levi-Kalisman, Y.; Regev, O. *Curr. Opin. Colloid. Interface Sci.* **2005**, *10*, 280–286.
(58) Attal, S.; Thiruvengadathan, R.; Regev, O. *Anal. Chem.* **2006**, *78*, 8098–8104.
(59) Moore, V. C.; Strano, M. S.; Haroz, E. H.; Hauge, R. H.; Smalley, R. E.; Schmidt, J.; Talmon, Y. *Nano Lett.* **2003**, *3*, 1379–1382.
(60) Xu, H.; Hong, R.; Wang, X.; Arvizo, R.; You, C.; Samanta, B.; Patra, D.; Tuominen, M. T.; Rotello, V. M. *Adv. Mater.* **2007**, *19*, 1383–1386.
(61) Mizutani, T.; Nosho, Y.; Ohno, Y. *J. Phys.: Conf. Ser.* **2008**, *109*, 012002.
(62) Soliveres, S.; Hoffmann, A.; Pascal, F.; Delseny, C.; Kabir, M. S.; Nur, O.; Salesse, A.; Willander, M.; Deen, J. *Fluctuation Noise Lett.* **2006**, *6*, L45—L55.

MA802147S